Astron. Astrophys. 319, 757–763 (1997)

ASTRONOMY
AND
ASTROPHYSICS

Beamed radio and far infrared emission in quasars and radio galaxies⋆

H. Hoekstra, P.D. Barthel, and R. Hes

Kapteyn Astronomical Institute, P.O. Box 800, 9700 AV Groningen, The Netherlands

Received 20 June 1996 / Accepted 28 August 1996

Abstract. Simple orientation model predictions for the radio to far infrared spectral energy distributions of radio-loud AGN are confronted with observations at various radio frequencies. This model is subsequently used to investigate 60 μm far-infrared data. The results are supportive of the unified scheme for Fanaroff-Riley class II radio galaxies and quasars. The relative strength of the beamed component is derived as a function of frequency, and it is found that the higher far infrared fluxes of quasars, as compared to radio galaxies, can be explained invoking moderately beamed nonthermal far-infrared emission.

Key words: galaxies: active – galaxies: jets – quasars: general – infrared: galaxies

1. Introduction

Active galaxies and Active Galactic Nuclei (AGN) show a wide variety of properties. Unified schemes (e.g., Antonucci, 1993) reduce the diversity of AGN by postulating that classes of objects are intrinsically the same and that their apparent differences are due to aspect dependent effects. As far as radio loud AGN are concerned, relativistic beaming phenomena provide an important motivation for such orientation related unification schemes. An additional key ingredient in the unified scheme of powerful Fanaroff-Riley class II (FR II) quasars and radio galaxies is an opaque dusty torus, surrounding the central accretion disk in its equatorial plane. This dust torus is believed to obscure the broad permitted emission lines and the strong optical nuclear continuum, when seen edge on, or equivalently, when observing a narrow line radio galaxy. Observing this torus more face on, allowing a clear sight line towards the central regions, the broad permitted lines will be seen, leading to classification as a quasar.

Send offprint requests to: P.D. Barthel

⋆ Data tables are only available in electronic form at the CDS via anonymous ftp to cdsarc.u-strasbg.fr (130.79.128.5) or via http://cdsweb.u-strasbg.fr/Abstract.html

On the assumption that the central engines of quasars and radio galaxies are indeed the same, the torus will intercept the same amount of nuclear radiation in both types of objects. Thus the torus will be heated and will re-emit photons at far infrared wavelengths. Under the condition of optically thin radiation, which is assumed to be longward of 50 μm (Draine, 1990), this far infrared emission will be isotropic.

Assuming then that long wavelength far infrared emission is due to thermal re-radiation by circumnuclear dust, quasars and radio galaxies are expected to show similar outputs of such radiation. It was claimed, however, that quasars are brighter than radio galaxies at 60 μm (Heckman et al., 1992, 1994; Hes et al., 1995 (Paper I hereafter)). Given this result, the radio loud unified model is in difficulty, if the radiation at 60 μm is indeed emitted isotropically. Several other explanations of the observations can be thought of, however. Pier and Krolik (1992) have shown that some level of anisotropy is always present due to optical thickness effects. In Paper I we argued that this effect cannot fully explain the observed behaviour of the 60 μm emission as a function of aspect angle. An alternative explanation, to be examined in this paper, is that the 60 μm emission is partly beamed non-thermal radiation from the central engine. We already showed in Paper I that the (normalized) 60 μm flux density shows proportionality to the radio core fraction, R. Since this R-parameter is considered to be a measure of relativistic jet orientation with respect to the line of sight, we argued in Paper I that far infrared beaming effects play a role. We here attempt to quantify these effects.

To this end we derive a model describing the effects of orientation dependent core radiation at radio frequencies. We subsequently show that such a model is also applicable to 60 μm observations for a sample of 3C/4C quasars and radio galaxies. Adopting the standard relativistic beaming formalism, and assuming that quasars and radio galaxies are linked by viewing angle dependence, we calculate the relative contributions of beamed and isotropic emission. These calculations imply a significant beamed 60 μm component from the nuclei of lobe dominated quasars and radio galaxies, in addition to the isotropic thermal dust component. We show that the magnitude of this

effect is such that it can account for the observed 60 μm emission as a function of aspect angle.

2. A simple orientation model

We derive a model in order to estimate the relative fractions of beamed and isotropic emission at several frequencies, including the 60 μm emission.

Fanaroff-Riley class II sources have a double lobed structure. A basic assumption in unified models for these objects is that they have two symmetrical, intrinsically similar jets. The flux of the approaching jet is boosted by a factor δ^ϵ due to geometrical beaming. Here δ is the Doppler boosting factor, given by:

$$\delta = \frac{1}{\gamma - \cos\theta\sqrt{\gamma^2 - 1}} \tag{1}$$

where γ is the usual Lorentz factor and θ is the angle between the line of sight and the direction of the jet. We assume that the value of the Doppler boosting factor does not change with frequency, i.e., γ and θ are taken constant with frequency. The value of ϵ is determined by jet geometry and composition (e.g., Begelman et al. 1984). We assume that ϵ is independent of frequency for the range in frequencies discussed in this paper. The value of ϵ, however, is allowed to differ from object to object. In addition to boosting, radiation from an approaching jet will be blue shifted by an extra factor δ. Let the Doppler boosting factor of the approaching jet be δ_{app} and the Doppler boosting factor of the receding jet δ_{rec}. If θ is the angle between the line of sight and the direction of the approaching jet, then δ_{rec} is given by Eq. (1) replacing θ by $180^\circ - \theta$. From Eq. (1) one can easily see that $\delta_{app} \geq 1$ and that $\delta_{rec} \leq 1$. The flux of the receding jet is 'boosted' by a factor δ_{rec}^ϵ. Furthermore, the emission of the receding jet is blue shifted by a factor δ_{rec}, which is effectively a redshift. Similarly, at angles approaching 90°, the emission of a high γ object will be low in comparison to a low γ object, due to forward flux boosting.

It is not possible to measure γ and θ directly. One can, however, measure the parameter R, which is defined as the ratio of core radio flux and the flux of the extended emission, in the object's restframe. This observable is a function of θ and γ (e.g., Orr & Browne 1982): radio sources oriented at small angles to the line of sight will display larger R-values than radio sources close to the sky plane, the magnitude of the effect being a strong function of γ. The usefulness of this R-parameter as orientation indicator has for instance been demonstrated by Kapahi & Murphy (1990) for the combined population of quasars and radio galaxies. It should be kept in mind, however, that intrinsic dispersion in core and lobe properties undoubtlessly contributes to the observed dispersion in R-values for extragalactic radio sources in general (e.g., Lonsdale & Barthel, 1987).

Here we use the value of the R-parameter from 5 GHz observations. Because the value of R has to be evaluated in the object's restframe, the observed flux densities have to be corrected for cosmological effects by means of a K-correction. However, as shown below, we find that the observed, uncorrected ratio of core and extended flux density at 5 GHz is more useful for this study. This ratio we will call Q. Radio sources having $Q > 1$ are core-dominated in the observed 5 GHz frame, whereas $Q < 1$ implies a lobe-dominated object. The relevant K-correction is approximately a multiplication by a factor $(1+z)^{-0.7}$, where we adopt $\alpha_{ext} - \alpha_c \approx 0.7$ as a representative value[1], where α_c is the spectral index of the core and α_{ext} the spectral index of the extended component (see Paper I). Hence $R \approx Q(1+z)^{-0.7}$.

Why these parameters Q and R are useful as orientation indicators can be seen from Eqs. (2) and (3) below. We assume that the extended (lobe) flux is emitted isotropically, and that the core emits both isotropic and beamed radiation.

It is found that when one includes isotropic 5 GHz core emission, this enters the model equations as the ratio of the isotropic and the extended flux density. Kapahi & Murphy (1990) found a typical 5 GHz value of $\log R \sim -3$ for radio galaxies, for which the radio axis is hypothesized to be close to the sky plane. This implies an upper limit of 0.001 on the ratio of isotropic core and extended flux at 5 GHz. We therefore will neglect isotropic core emission at 5 GHz and assume that the core emission at this frequency is purely beamed radiation. For the observed flux density of the extended emission at 5 GHz (F_5^{ext}) we can thus write:

$$F_5^{ext} = S_5^{ext}(1+z)^{-\alpha_5^{ext}} \tag{2}$$

where S_5^{ext} is the flux density at 5 GHz of the extended emission in the object's restframe, and

$$F_5^{beam} = S_5^{beam}(\delta_{app}^{\epsilon+1} + \delta_{rec}^{\epsilon+1})(1+z)^{-\alpha_c} \tag{3}$$

where S_5^{beam} is a measure of the flux density (in the restframe) of the central engine, when its emission would not be beamed. In this paper observed flux densities are denoted by the symbol F, whereas intrinsic values are denoted by the symbol S. When we divide Eq. (3) by (2), we find that $(\delta_{app}^{\epsilon+1} + \delta_{rec}^{\epsilon+1})$ can be written in terms of R or Q and intrinsic parameters:

$$\begin{aligned}(\delta_{app}^{\epsilon+1} + \delta_{rec}^{\epsilon+1}) &\simeq \frac{S_5^{ext}}{S_5^{beam}} R \\ &\simeq \frac{S_5^{ext}}{S_5^{beam}} Q(1+z)^{\alpha_c - \alpha_5^{ext}}\end{aligned} \tag{4}$$

Since there is a range in emitted power for FR II sources, it is useful to 'normalize' the emission of different objects. This normalization allows a fair comparison of the most luminous objects with less luminous objects. We therefore will normalize the flux densities by the extended isotropic 178 MHz radio lobe emission. This optically thin radiation is a reasonably good measure of the actual AGN power (Hes et al. 1993, McCarthy 1993).

We now address the dependence of the flux density at any radio frequency ν as a function of Q. We assume that the emission at this frequency consists of two components: a beamed

[1] Throughout this paper we adopt flux density proportional to $\nu^{-\alpha}$

component and a component that is emitted isotropically. For the observed flux density at frequency ν we can write:

$$F_\nu^{tot} = S_\nu^{beam}(\delta_{app}^{\epsilon+1} + \delta_{rec}^{\epsilon+1})(1+z)^{-\alpha_c} + S_\nu^{iso}(1+z)^{-\alpha_\nu^{iso}} \quad (5)$$

which is just the sum of Eqs. (2) and (3) for arbitrary frequency ν. This result can be normalized with the observed 178 MHz flux density, given by:

$$F_{178} = S_{178}(1+z)^{-\alpha_{178}} \quad (6)$$

When we divide equation (5) by (6) we obtain for the ratio F_ν^{total}/F_{178}:

$$\begin{aligned}\frac{F_\nu^{tot}}{F_{178}} &= BD_\nu R(1+z)^{\alpha_{178}-\alpha_c} + \frac{S_\nu^{iso}}{S_{178}}(1+z)^{\alpha_{178}-\alpha_\nu^{iso}} \\ &= BD_\nu Q(1+z)^{\alpha_{178}-\alpha_5^{ext}} + \frac{S_\nu^{iso}}{S_{178}}(1+z)^{\alpha_{178}-\alpha_\nu^{iso}}\end{aligned} \quad (7)$$

where we have defined B as the ratio of S_5^{ext} and S_{178}, and where D_ν is defined as the ratio between S_ν^{beam} and S_5^{beam}. D_ν therefore measures the strength of the beamed component, at frequency ν, relative to the 5 GHz value, hence the beamed component spectrum. When we assume that the spectral index of the isotropic emission does not change much with frequency, i.e. $\alpha_{178} \approx \alpha_5^{ext} \approx \alpha_\nu^{iso}$ and adopting $\alpha_{178} = 0.7$ and $\alpha_c = 0$, we find:

$$\begin{aligned}\frac{F_\nu^{tot}}{F_{178}} &= BD_\nu \left[R(1+z)^{0.7} + C_\nu\right] \\ &= BD_\nu \left[Q + C_\nu\right]\end{aligned} \quad (8)$$

where we define C_ν as $S_\nu^{iso}/(S_5^{ext}D_\nu)$. From this we see that Q is the most useful parameter, because all redshift corrections have vanished.

Eq. (8) is a model expression for the spectral slope at frequency ν with respect to the isotropic 178 MHz emission, as function of the measured 5 GHz core fraction, Q. It describes the normalized spectral energy distribution (SED) as sum of an isotropic SED and a variable core SED, the strength of the latter governed by Q. Although equation (8) has been derived from the relativistic beaming formalism, it can also simply be derived adding isotropic extended and isotropic core emission, both having their own spectral slopes, with Q as a free parameter.

We will proceed by fitting the model to observations, with C_ν and D_ν as free parameters. As mentioned above, D_ν is a relative measure of the beam (or core) strength. C_ν is a measure of the value of R or Q where core radiation starts dominating the energy output: a low value of C_ν implies that beamed or isotropic core radiation will be important already at moderate R or Q vales, for that particular frequency. In Sect. 4 we will confront this simple model with radio data taken from the literature.

3. Data

To test the validity of the inferred orientation model, we confront it with data taken from the literature. We use samples of FR II radio galaxies and quasars, which are presented in Tables 1, 2, and 3, available in electronic form. The radio galaxies, which are listed in Table 1, have all been taken from the 3CR catalogue (Spinrad et al., 1985 and updates). We included all radio galaxies for which reliable values for the 5 GHz core fraction Q are available. We have assembled 178, 318, 408, 750, 1400, 2700, 5000, 10695 and 14900 MHz flux density values from the literature. In addition, values for the 60 μm far-infrared flux density were taken from IRAS data assembled in Paper I.

Table 2 subsequently contains 3CR quasars with known Q-values. Reliable model fits require a good coverage of the core fraction, Q. Objects with high values for Q are relatively rare in low frequency selected samples such as 3CR. In fact only the quasars 3C 345 and 3C 454.3 have $Q > 1$. Therefore, in order to obtain a good sampling for large Q, we extended the sample with 4C quasars known to have large values for Q. These objects are listed in Table 3. The only reason to include these quasars is to obtain a good sampling of the high Q region. This procedure could introduce a selection effect. There are, however, no indications that the values of F_ν/F_{178} for FR II objects from the 4C catalogue differ from the values for 3C objects. For completeness one should include also low Q objects from the 4C catalogue, but this would not change our results for the low Q region. It is important to realize that the F_{178}-values in the tables are those for the *extended, unbeamed, non-core* emission. In several cases we have extrapolated the (assumed flat-spectrum) GHz core spectrum to 178 MHz and subtracted this value in order to obtain the relevant isotropic component. Generally speaking, the 4C quasars have (isotropic) radio luminosities between 0.1 and 0.5 of the values for the 3C objects. As can be seen in Fig. 1, the few included 4C quasars that have intermediate Q-values are distributed in the same region as 3C quasars with comparable values of Q. We therefore feel certain that our results do not suffer from selection effects.

The radio data are available in electronic format at the CDS, and were mostly taken from Kühr et al. (1981), with additions from Kellermann et al. (1969) and Large et al. (1981). 5 GHz core flux density values (used to determine Q-values) were taken from Paper I. For galaxies that are not listed in Paper I, we have taken 5 GHz core flux density values from Giovannini et al. (1988). For 3C quasars which do not appear in Paper I, we used data from Akujor et al. (1991), Bridle et al. (1994), Foley and Barthel (1990), Jenkins, Pooley and Riley (1977), Lonsdale, Barthel and Miley (1993), and Riley and Pooley (1975). For 4C quasars which do not appear in Paper I, we used (radio) data from Murphy et al. (1993), O'Dea et al. (1988), Owen & Puschell (1984), Reid et al. (1995), and Saikia et al. (1984, 1989).

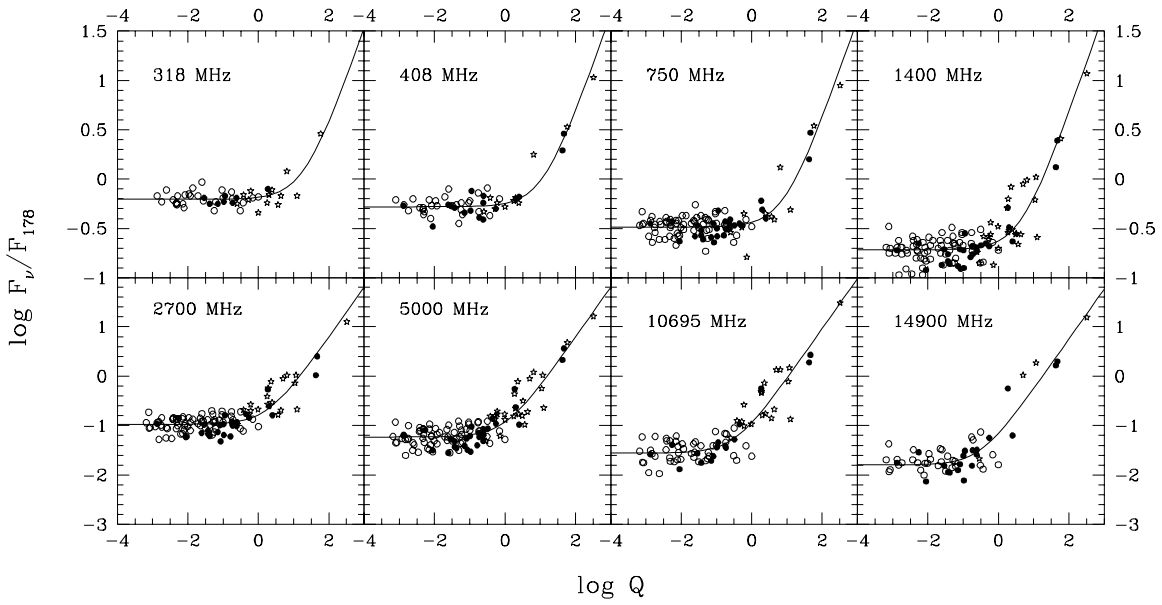

Fig. 1. Plot of $\log(F_\nu^{tot}/F_{178\mathrm{MHz}})$ versus $\log\ Q$ for 318, 408, 715, 1400, 2700, 5000, 10695 and 14900 MHz. Open circles represent 3C radio galaxies, filled circles 3C quasars and stars denote 4C quasars. The solid lines are least square fits to the data.

4. Confronting the data

Using the data from the previous section, we confront the model from Sect. 2 with the observations. In Fig. 1 we have plotted the ratios F_ν/F_{178} versus Q, with open circles representing 3C radio galaxies, filled circles 3C quasars, and stars 4C quasars. The objects appear in fairly narrow bands, indicating that the normalization works well. There is a continuous trend from the low Q objects, i.e., radio galaxies, to the high Q objects, i.e., quasars. These plots, including the fact that there is substantial overlap in the intermediate Q-range for the two populations, therefore constitute important evidence that radio-loud quasars may well be unified with radio galaxies (Scheuer 1987, Peacock 1987, Barthel 1989). An alternative explanation, attributing the more prominent quasar cores to a higher level of activity will be discussed below.

The best frequency to start the model fit is 5 GHz, because at this frequency both C_ν and D_ν are equal to unity. Eq. (8) then reads:

$$\frac{F_5^{tot}}{F_{178}} = B(Q+1)$$

A least squares fit of the model to the data is shown in Fig. 1. This fit results in a value of -1.2 for $\log\ B$, which is equivalent to the statement $\alpha_{178\ \mathrm{MHz}}^{5\ \mathrm{GHz}} = 0.83$ for the extended radio lobe emission, quite consistent with values obtained for larger samples (e.g., Kellermann et al. 1969). When we fit the model to the data, taking C_5 as a free parameter as well, we obtain a comparable fit. This result indicates that our model represents the 5 GHz observations well. The assumptions made in the derivation of the model therefore seem acceptable.

Table 4. Results of least squares fits of the model of Sect. 2 to the observations. In column (1) the frequency used is given; col. (2) lists the value for C_ν; col. (3) the value for $\log D_\nu$; col. (4) the value for S_ν^{beam}/S_5^{beam} (D_ν); col (5) the value for S_ν^{iso}/S_5^{ext} $(C_\nu D_\nu)$.

ν [MHz]	C_ν	$\log D_\nu$	$\frac{S_\nu^{beam}}{S_5^{beam}}$	$\frac{S_\nu^{iso}}{S_5^{ext}}$
(1)	(2)	(3)	(4)	(5)
318	20.2	-0.28	0.52	10.5
408	12.3	-0.14	0.72	8.9
750	8.6	-0.19	0.65	5.6
1400	4.3	-0.12	0.76	3.3
2700	1.8	0.0	1.0	1.8
5000	1.0	0.0	1.0	1.0
10695	0.32	0.17	1.5	0.48
14900	0.30	-0.04	0.91	0.27

We proceed by fitting the model to the data at the other frequencies listed in the data tables. With reference to Fig. 1, the results of the least squares model fits are listed in Table 4. We used the value of $\log B = -1.2$ to calculate the values of D_ν.

Although the data for high values of Q at some frequencies are sparse, we see in Fig. 1 that the simple model of Sect. 2 provides a good fit to the data. It can be clearly seen that the fraction of isotropic, i.e. Q-independent radiation becomes progressively smaller with increasing frequency. The plots shown in Fig. 1, show that the scatter increases with increasing frequency. This effect is clearest visible in the flat part, i.e. for low values of Q. Scatter in the spectral indices seems to be the most important source of scatter. In the derivation of the model we neglected changes in the spectral index α_ν^{iso} with frequency.

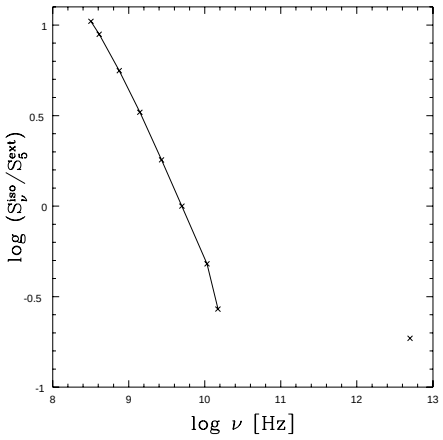

Fig. 2. Plot of log $(C_\nu D_\nu)$ = log(S_ν^{iso}/S_5^{ext}) versus log ν. Crosses are the results of the model fits listed in Table 4. The right most point is the result of fitting the model to 60 μm observations.

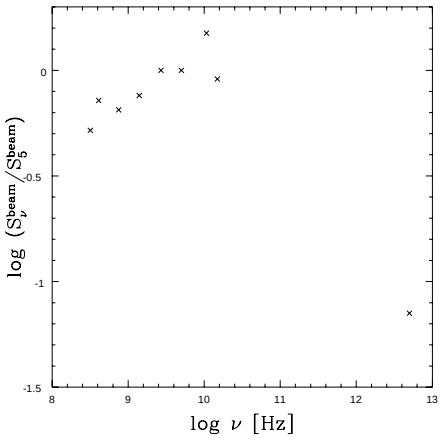

Fig. 3. Plot of logD_ν = log$(S_\nu^{beam}/S_5^{beam})$ versus log ν. Crosses are the results of the model fits listed in Table 4. The right most point is the result of fitting the model to 60 μm observations. A fairly flat beamed component spectrum with rapid turnover to far-infrared wavelengths is seen.

Furthermore, the spectral indices can change from object to object.

By fitting the model to 5 GHz data, we found a value of -1.2 for log B. Assuming $F_\nu = F_o\nu^{-\alpha}$ and $\alpha_{178} = \alpha_5^{ext} = 0.7$, one would expect a value of -1.01 for log B. An increase of the mean spectral index from 178 MHz to 5 GHz of approximately 0.13 can explain the value we found in the least squares model fit. This is in agreement with the earlier mentioned value of 0.83 for $\alpha_{178\mathrm{MHz}}^{5\mathrm{GHz}}$. Such radio spectral index steepening effects, which are generally attributed to synchrotron losses (e.g., Pacholczyk 1977) will introduce scatter.

In Fig. 2 we have plotted the ratio S_ν^{iso}/S_5^{ext} as a function of frequency. The powerlaw dependence of this ratio as well as the spectral steepening are clearly visible. In Fig. 2 we also plotted the result for the 60 μm observations. The confrontation of the model with 60 μm observations is discussed in Sect. 5.

From Table 4, we find that the spectrum of the beamed component increases from lower to higher frequencies and reaches a maximum around 10.7 GHz. Its variation with radio frequency is however relatively small. This is also expected from the observational fact that the cores of radio galaxies and quasars usually show flat spectra. In Fig. 3, we plot S_ν^{beam}/S_5^{beam} as a function of ν. The 'flat' spectrum of the central engine is in good agreement with observations. In Fig. 3 the 60 μm point is also shown. The results for the 60 μm emission are discussed in Sect. 5.

Since we assumed that the Doppler boosting was frequency independent, Fig. 3 should also represent the observed radio spectrum of an average beamed radio core, i.e., blazar. Good agreement with actual observations (e.g., Bregman et al. 1986, Impey & Neugebauer 1988) is seen: $\alpha_{1\mathrm{GHz}} \sim -0.25$ with a pronounced turnover at 10^{10} Hz. As mentioned at the end of Sect. 2, beaming is not explicitly required in the model derivation. Hence Fig. 3 should also represent the core spectrum of the average FR II radio source, irrespective of the mechanism involved in producing this core spectrum. We note with interest that the inferred peak at 10^{10} Hz is indeed observed in the well sampled Cygnus A core spectrum (Salter et al. 1989), and that

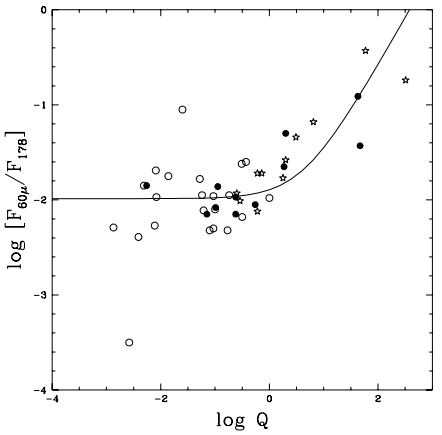

Fig. 4. Plot of log$(F_{60\mu}^{tot}/F_{178\mathrm{MHz}})$ versus log Q. Open circles represent 3C radio galaxies, filled circles 3C quasars and stars denote 4C quasars. The solid line is a least square fit to the data.

such peaked core spectra are typically observed (Rudnick et al. 1986).

5. Beamed 60 μm emission

Having quantified the frequency dependent level of core beaming at radio wavelengths, we proceed by addressing the issue of beaming at far infrared wavelengths, applying the formalism derived in this paper to 60 μm observations. In Paper I it was already suggested that beamed far infrared emission from the core might explain the higher far infrared fluxes of quasars compared to radio galaxies (Paper I; Heckman et al. 1992, 1994).

In Fig. 4 we have plotted the ratio $F_{60\mu}^{tot}/F_{178\mathrm{MHz}}$ versus Q. In this figure also the least squares model fit (solid line) is shown. We see that the model can fit the observations well. To obtain this fit, we excluded the two outlying points, corresponding to 3C405 (too low) and 3C231 (too high). 3C405 (Cygnus A) is known

to have extremely bright radio lobes, implying a high 178 MHz flux density. Due to confinement by an unusually dense intracluster environment, its radio luminosity is roughly 1.5 orders of magnitude higher than for sources of comparable redshift (Barthel & Arnaud 1996). 3C231 (M 82), which has an excessive far infrared output compared to the 178 MHz emission, is a well known starburst galaxy with radio emission coming from supernova remnants rather than from a classical double radio structure (Muxlow et al. 1994).

We proceed by inferring the parameters quantifying the anisotropic 60 μm component. The assumptions $\alpha_{core} = 0$ and $\alpha_{\nu}^{iso} = 0.7$ are valid in the radio regime but certainly not at far infrared frequencies. Blazar studies have shown that $\alpha_{core} \sim 1.25$ in the far infrared (e.g., Impey & Neugebauer 1988), while the spectral index of extended, isotropic 60 μm emission typically has $\alpha \approx 1.0$ (e.g., Neugebauer et al. 1986). Therefore the K-corrections in the derivations of Eqs. (7) and (8) do not vanish anymore. In fact, eq.(8) at far infrared wavelengths transforms to

$$\frac{F_{60\mu}^{tot}}{F_{178}} = BD_{60\mu}^{*}\left[Q + C_{60\mu}^{*}\right] \tag{9}$$

where $D_{60\mu}^{*} = D_{60\mu}(1+z)^{-1.25}$ and $C_{60\mu}^{*} = C_{60\mu}(1+z)^{0.95}$, using the spectral indices mentioned above.

The least squares model fit to the data in Fig. 4 then yields $C_{60\mu}^{*} = 4.2$ and $D_{60\mu}^{*} = 0.042$, respectively. Solving for the average values $\langle(1+z)^{-1.25}\rangle$ and $\langle(1+z)^{0.95}\rangle$ of the 60 μm detected objects leads to $C_{60\mu} = 2.6$ and $D_{60\mu} = 0.071$, which values are plotted in Figs. 2 and 3.

Thus we find that the strength of the beamed component at 60 μm, relative to the 5 GHz emission, is relatively weak, but nonzero. Although this component is much weaker than in the radio, these results indicate that one cannot neglect nonthermal far infrared emission for objects where the beam is approaching the line of sight, or – in the isotropic model – where the core fraction is substantial. We conclude that the far infrared output of quasars is enhanced. This effect can explain the high 60 μm output of quasars that have values for log Q in excess of 0.5.

It is straightforward to calculate the relative contribution of the Q-dependent radiation to the total far infrared emission. This fraction f as a function of Q and z is given by:

$$f_{60} = \frac{Q}{Q + C_{60\mu}(1+z)^{0.95}} \cdot 100\% \tag{10}$$

which is the ratio of $F_{60\mu}^{beam}$ and $F_{60\mu}^{total}$. In Fig. 5 we plot $f_{60}(Q,z)$ at 60 μm, using $C_{60\mu} = 2.6$ and $z = 0$ (solid line). The dashed lines in this figure correspond to values of 1.2 and 4.9 for $C_{60\mu}$, which are the values that define the envelope around the points in Fig. 4. Note that $Q = R$, at $z = 0$. From the equation for $f_{60}(Q,z)$ it is easily seen that these lines represent the upper envelope to the beamed 60 μm fraction: the curves for $z > 0$ objects will be below the plotted ones.

The fraction of beamed 60 μm radiation is seen to increase rapidly from log $Q = -1$ to log $Q = 1$, for nearby objects. For objects having log $Q = 0$, i.e., equal flux densities in core and lobes, 20% to 50% of their total 60 μm emission is beamed. At redshifts up to 1, this fraction is still some tens of percent. It is therefore likely that the far infrared detected objects with log $Q \approx 0$ are those with a relatively large beamed contribution. It should be kept in mind that most 60 μm detections of 3C quasars were just above the IRAS detection limit (e.g., Fig. 1 in Paper I).

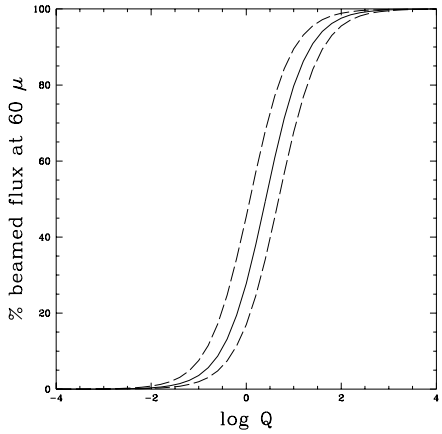

Fig. 5. Plot of the observed fraction of beamed 60μm far infrared emission as function of the observed 5 GHz fractional core flux density, Q. The solid line corresponds to $C_{60\mu}$=2.6 at $z = 0$, the dashed curves correspond to $C_{60\mu}$=1.2 and 4.9, from left to right. These lines represent the upper envelope to the fraction of beamed 60 μm emission.

Although Q is a good measure of the orientation of the beam with respect to the line of sight, for some objects it might not be so. An example is 3C351, a quasar with a relatively weak radio core (log $Q = -2.3$). Such a value normally corresponds to a radio galaxy. Therefore some of the detected quasars with fairly low values of Q, might in fact have a larger fraction of far infrared emission than is expected from their value of Q.

As indicated in Paper I, anisotropic emission of the dust torus (Pier & Krolik, 1992) can enhance the far infrared output. This process cannot fully explain the strong increase of far infrared emission as a function of Q. For objects that have intermediate values for log Q, between -1 and 0.5, this effect, however, might be important. Thus the combination of an anisotropic emitting dust torus and beamed far infrared radiation might explain the observed higher far infrared output of quasars compared to radio galaxies (Paper I; Heckman et al. 1992, 1994). We are currently pursuing sensitive ISO photometry in order to address this issue further.

As discussed above, the radio and FIR data do not *require* the relativistic beaming mechanism, but are consistent with it. The data are also consistent with radio galaxies and quasars having isotropic core radiation with a spectrum as shown in Fig. 3. This core emission then becomes progressively stronger with increasing 5 GHz core fraction, at a fixed spectral shape. Given the various lines of evidence, suggesting that the core fraction Q is a measure of beam/source orientation (e.g., Hough & Readhead 1989, Bridle et al. 1994), we think that the beaming mechanism is the likely cause behind the good model fits. We cannot

exclude the possibility of the combination of isotropic core radiation and evolution of core strength, however, but such an evolutionary model should then be able to explain the observed fixed spectral shape of the core component.

Finally, Fig. 2 makes immediately clear that the isotropic 60 μm emission and the isotropic radio emission must have a different origin. While the latter is lobe synchrotron radiation, the former should certainly not be identified with that mechanism (Paper 1). A thermal, circumnuclear dust origin (Sanders et al. 1989) is considered the most likely.

6. Conclusion

A simple model can attribute the shape of the radio–FIR spectral energy distribution in Fanaroff-Riley class II radio galaxies and quasars to a combination of isotropic and beamed radiation. The model allows the spectral energy distributions of both the isotropic and the beamed component to be determined. The results are furthermore supportive of the unified scheme for FR II radio galaxies and quasars. Whereas isotropic core emission cannot be ruled out, that explanation – adopting evolving core strength – seems contrived. By confronting the model with far infrared data we find that even at 60 μm a nonthermal core component contributes significantly in quasars. The scatter however indicates that – besides uncertain K-corrections – also other processes like starbursts or an anisotropically emitting torus contribute to the far infrared output.

References

Akujor, C.E., Spencer, R.E., Zhang, F.J., et al.: 1991, MNRAS, 250, 215

Antonucci, R.: 1993, ARA&A, 31, 473

Barthel, P.D.: 1989, ApJ, 336, 606

Barthel, P.D., Arnaud, K.A.: 1996, MNRAS, in press

Begelman, M.C., Blandford, R.D., Rees, M.J.: 1984, Rev. Mod. Phys, 56, 255

Bregman, J.N., Glassgold, A.E., Huggins, P.J., et al.: 1986, ApJ, 301, 708

Bridle, A.H., Hough, D.H., Lonsdale, C.J., Burns, J.O., Laing, R.A.: 1994, AJ, 108, 766

Draine, B.T.: 1990 in: *The Interstellar Medium in Galaxies*, eds. H.A. Thronson and J.M. Shull, Kluwer, Dordrecht, 483

Foley, A.R., Barthel, P.D.: 1990, A&A, 228, 17

Giovannini, G., Feretti, L., Gregorini, L., Parma, P.: 1988, A&A, 199, 73

Heckman, T.M., Chambers, K.C., Postman, M.: 1992, ApJ, 391, 39

Heckman, T.M., O'Dea, C.P., Baum, S.A., Laurikainen, E.: 1994, ApJ, 428, 65

Hes, R., Barthel, P.D., Fosbury, R.A.E.: 1993, Nat, 362, 326

Hes, R., Barthel, P.D., Hoekstra, H.: 1995, A&A, 303, 8 (Paper I)

Hough, D.H., Readhead, A.C.S.: 1989, AJ, 98, 1208

Impey, C.D., Neugebauer, G.: 1988, AJ, 95, 307

Jenkins, C.J., Pooley, G.G., Riley, J.M.: 1977, MemRAS, 84, 61

Kapahi, V.K., Murphy, D.W.: 1990 in: *Parsec-scale Radio Jets*, eds. J.A. Zensus & T.J. Pearson, Cambridge, CUP, 313

Kellermann, K.I., Pauliny-Toth, I.I.K., Williams, P.J.S.: 1969, ApJ, 157, 1

Kühr, H., Nauber, U., Pauliny-Toth, I.I.K., Witzel, A. 1981, *A Catalogue of Radio Sources*, MPIfR preprint 55

Large, M.I., Mills, B.Y., Little, A.G., Crawford, D.F., Sutton, J.M.: 1981, MNRAS, 194, 693

Lonsdale, C.J., Barthel, P.D.: 1987, AJ, 94, 1487

Lonsdale, C.J., Barthel, P.D., Miley, G.K.: 1993, ApJS, 87, 63

McCarthy, P.J.: 1993, ARA&A, 31, 639

Murphy, D.W., Browne, I.W.A., Perley, R.A.: 1993, MNRAS, 264, 298

Muxlow, T.W.B., Pedlar, A., Wilkinson, P.N., et al.: 1994, MNRAS, 266, 455

Neugebauer, G., Miley, G.K., Soifer, B.T., Clegg, P.E.: 1986, ApJ, 308, 815

O'Dea, C.P., Barvainis, R., Challis, P.M.: 1988, AJ, 96, 435

Orr, M.J.L., Browne, I.W.A.: 1982, MNRAS, 200, 1067

Owen, F.N., Puschell, J.J.: 1984, AJ, 89, 932

Pacholczyk, A.G.: 1977, *Radio Galaxies*, Pergamon Press, New York

Peacock, J.A.: 1987 in: *Astrophysical Jets and their Engines*, ed. W. Kundt, Kluwer, Dordrecht, 185

Pier, E.A., Krolik, J.: 1992, ApJ, 401, 99

Reid, A., Shone, D.L., Akujor, C.E., et al.: 1995, A&AS, 110, 213

Riley, J.M., Pooley, G.G.: 1975, MemRAS, 80, 105

Rudnick, L., Jones, T.W., Fiedler, R.: 1986, AJ, 91, 1011

Saikia, D.J., Shastri, P., Sinha, R.P., Kapahi, V.K., Swarup, G.: 1984, JA&A, 5, 429

Saikia, D.J., Shastri, P., Cornwell, T.J., Junor, W., Muxlow, T.W.B.: 1989, JA&A, 10, 203

Salter, C.J., Chini, R., Haslam, C.G.T., et al.: 1989, A&A, 220, 42

Sanders, D.B., Phinney, E.S., Neugebauer, G., Soifer, B.T., Matthews, K.: 1989, ApJ, 347, 29

Scheuer, P.A.G.: 1987 in: *Superluminal Radio Sources*, ed. J.A. Zensus & T.J. Pearson, Cambridge, CUP, 104

Spinrad, H., Djorgovski, S., Marr, J., Aguilar, L.: 1985, PASP, 97, 932

This article was processed by the author using Springer-Verlag LaTeX A&A style file *L-AA* version 3.